PERGAMON

International Journal of Heat and Mass Transfer 42 (1999) 2085–2099

International Journal of HEAT and MASS TRANSFER

# Heat transfer in gravity-driven film flow of power-law fluids

D.-Y. Shang[1], H.I. Andersson*

*Division of Applied Mechanics, Faculty of Mechanical Engineering, The Norwegian University of Science and Technology, N-7034 Trondheim, Norway*

Received 12 February 1998

**Abstract**

A mathematical model for the flow and heat transfer in an accelerating liquid film of a non-Newtonian power-law fluid is presented. The thermal boundary layer equation permits exact similarity solutions only in the particular case when the power-law index $n$ is equal to unity, i.e. for Newtonian films. To this end, the heat transfer problem is solved by means of a local nonsimilarity approach with $n$ and local Prandtl number $Pr_x$ being the only parameters. A critical Prandtl number $Pr_x^*$ is introduced, which is a monotonically increasing function of $n$. The nonsimilar heat transfer problem is integrated numerically for several parameter combinations in the ranges $0.2 \leqslant n \leqslant 2.0$ and $0.001 \leqslant Pr_x \leqslant 1000$ and the calculations for $n = 1$ compared favourably with earlier results for Newtonian liquid films. For high Prandtl numbers, the temperature gradient at the wall is controlled by the wall gradient of the streamwise velocity component, which is practically independent of $n$ for dilatant fluids ($n > 1.0$) but increases significantly with increasing pseudo-plasticity ($n < 1.0$). For $Pr_x \ll 1$, on the other hand, the wall gradient of the temperature field increases slowly with $n$ and this modest variation is ascribed to the displacement effect caused by the presence of the momentum boundary layer. Curve-fit formulas for the temperature gradient at the wall are provided in order to facilitate rapid and yet accurate estimates of the local heat transfer coefficient and the Nusselt number. 

**Nomenclature**

$a$ thermal diffusivity $\lambda/\rho c_p$ [$m^2\ s^{-1}$]
$c_p$ specific heat [$J^{-1}\ (kg^{-1}\ K^{-1})$]
$g$ gravitational acceleration [$m\ s^{-2}$]
$g(\eta, \xi)$ subsidiary variable, $\partial\theta(\eta, \xi)/\partial\xi$
$h(\eta, \xi)$ subsidiary variable $\xi \cdot g(\eta, \xi)$
$K$ coefficient of consistency [$kg\ s^{n-2}\ m^{-1}$]
$L$ characteristic streamwise length [m]
$n$ power-law index
$Nu_x$ local Nusselt number, $\alpha_x x/\lambda$
$Pr_x$ local Prandtl number, equation (20)
$Pr_x^*$ critical local Prandtl number
$q_x$ local heat transfer rate [$W\ m^{-2}$]
$Re_x$ local Reynolds number, $x^n(w_{x,\infty})^{2-n}\rho/K$, in equation (10)
$t$ temperature [K]
$w_x$, $w_y$ velocity in $x$- and $y$-direction, respectively [$m\ s^{-1}$]
$W_x(\eta)$, $W_y(\eta)$ dimensionless velocity components in $x$- and $y$-direction, respectively
$x$, $y$ streamwise and cross-stream co-ordinates [m].

*Greek symbols*

$\alpha$ angle of inclination
$\alpha_x$ local heat transfer coefficient [$W\ m^{-2}\ K^{-1}$]
$\delta$ thickness of boundary layer [m]
$\eta$ dimensionless co-ordinate $(y/x)(Re_x)^{1/(n+1)}$ in equation (8)
$\eta_{\delta_l}$ dimensionless thickness of momentum boundary layer
$\eta_{\delta_t}$ dimensionless thickness of thermal boundary layer
$\theta$ dimensionless temperature in equation (13)
$\lambda$ thermal conductivity [$W\ m^{-1}\ K^{-1}$]
$\xi$ dimensionless co-ordinate, $x/L$, in equation (9)
$\rho$ density [$kg\ m^{-3}$].

*Subscripts*

l momentum boundary layer

* Corresponding author. Tel.: 00 47 7359 3556; fax: 00 47 7359 3491; e-mail: helge.i.andersson@mtf.ntnu.no

[1] Present address: School of Mechanical and Materials Engineering, Washington State University, Pullman, WA 99160-2920, U.S.A.

0017–9310/99/$ - see front matter 
PII: S0017–9310(98)00301–9

t thermal boundary layer
w wall condition
$x$ local value
$\infty$ free stream condition.

## 1. Introduction

Efficient heating or cooling of liquids can be achieved by allowing the fluid to flow in a thin film along a solid surface kept at a constant temperature. While the hydrodynamics of thin film flows of Newtonian liquids has been extensively studied for several decades [1], only modest attention has been devoted to gravity-driven films of non-Newtonian liquids.

Fully developed laminar film flow along an inclined plane was considered by Astarita et al. [2], who measured the film thickness for various inclinations and flow rates. In a similar investigation by Therien et al. [3], experimental data for the film thickness were compared with an analytic expression for the thickness of fully developed films of power-law fluids. Sylvester et al. [4] compared predicted and experimental hydrodynamical characteristics for wavy but otherwise fully developed films of power-law and Newtonian liquids.

The hydrodynamics of developing power-law films has been studied by means of the integral method approach [5–10] and similarity analysis [11, 12]. Yang and Yarbrough [5, 6] and Narayana Murthy and Sarma [7] extended the conventional analysis for Newtonian films to also include power-law fluids. Later, Narayana Murthy and Sarma [8] included the effect of interfacial drag at the liquid–vapour interface in a similar analysis while Tekic et al. [9] presented results which accounted for the streamwise pressure gradient and surface tension and Andersson and Irgens [10] explored the influence of the rheology of the film on the hydrodynamic entrance length. A different approach was adopted by Andersson and Irgens [11, 12], namely to divide the accelerating film flow into a developing viscous boundary layer and an external inviscid freestream, as depicted in Fig. 1. They furthermore demonstrated that a similarity transformation exists, such that the boundary layer momentum equation for power-law fluids is exactly transformed into a Falkner–Skan type ordinary differential equation.

More recently, the present authors [13] proposed an alternative similarity transformation for studies of the hydrodynamics of gravity-driven power-law films. This new transformation was an extension of the dimensionless velocity component approach introduced by Shang and Wang [14] for Newtonian boundary layers and employed successfully to free convection [14, 15], film boiling [16] and condensation [17] with the particular view to account for the variability of the thermophysical properties of the fluid.

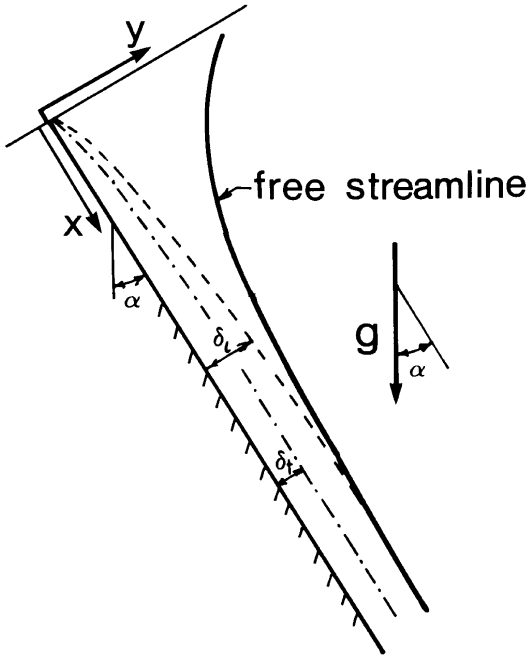


Fig. 1. Schematic representation of accelerating film flow.

The heat transfer from a constant temperature wall to hydrodynamically fully developed power-law films was probably first considered by Yih and Lee [18], while the corresponding mass transfer problem (i.e. solid dissolution from the wall and diffusion into the film) has been studied by Astarita [19] and Mashelkar and Chavan [20].

However, for accelerating film flow, the heat transfer coefficient for the inlet section is considerably higher than further downstream [21]. To the authors' knowledge, the integral method approach by Narayana Murthy and Sarma [22] and the approximate analysis of Andersson [23] are the first and only approaches to the important problem of heat transfer to developing non-Newtonian films.

The objective of the present paper is to consider the heat transfer to a gravity-driven power-law film accelerating along an inclined wall. This study is a natural extension of our recent analysis [13] of the hydrodynamics of a developing power-law film. It is our intention to take advantage of the new similarity transformation proposed in that study and develop a rigorous mathematical model for the accompanying heat transfer problem. The controlling dimensionless parameters will be identified and accurate numerical solutions will be presented for a number of different parameter combinations. Finally, on the basis of the numerical results, a short-cut method for rapid and yet reliable estimates of the heat transfer rate will be provided.

## 2. Physical model and governing partial differential equations

Consider the accelerating laminar flow of a non-Newtonian liquid film down along an inclined plane surface, as shown schematically in Fig. 1. The incompressible and inelastic fluid is assumed to obey the Ostwald–de-Waele power-law model and the action of viscous stresses is confined to the developing momentum boundary layer region adjacent to the solid surface. The basic boundary layer equations for mass, momentum and thermal energy are:

$$\frac{\partial w_x}{\partial x}+\frac{\partial w_y}{\partial y}=0 \tag{1}$$

$$w_x\frac{\partial w_x}{\partial x}+w_y\frac{\partial w_x}{\partial y}=g\cos\alpha+n\frac{K}{\rho}\left(\frac{\partial w_x}{\partial y}\right)^{(n-1)}\frac{\partial^2 w_x}{\partial y^2} \tag{2}$$

$$w_x\frac{\partial t}{\partial x}+w_y\frac{\partial t}{\partial y}=\frac{\lambda}{\rho c_p}\frac{\partial^2 t}{\partial y^2} \tag{3}$$

with boundary conditions

$$y=0:\quad w_x=0,\quad w_y=0,\quad t=t_w \tag{4}$$

$$y\to\delta_l\quad w_x\to w_{x,\infty} \tag{5}$$

$$y\to\delta_t\quad t\to t_\infty \tag{6}$$

where $w_x$ and $w_y$ are velocity components in the $x$- and $y$-directions, respectively, whereas $g$ and $\alpha$ denote the gravitational acceleration and the angle of inclination of the plane wall. Here, it has been anticipated that $(\partial w_x/\partial y)\geqslant 0$ throughout the entire film. $\delta_l$ and $\delta_t$ are momentum and thermal boundary layer thicknesses, respectively, whereas $w_{x,\infty}$ and $t_\infty$ denote the velocity and temperature of the fluid outside the respective boundary layers. It is noteworthy that while $w_{x,\infty}$ varies with $x$, the external temperature $t_\infty$ as well as the wall temperature $t_w$ are constants. The fluid properties $\lambda$, $\rho$, $c_p$, $K$ and $n$, which are assumed to be constant in the present analysis, are the thermal conductivity, density, specific heat, coefficient of consistency and power-law index, respectively. The deviation of $n$ from unity indicates the degree of deviation from Newtonian rheology and the particular case $n=1$ represents a Newtonian fluid with dynamic coefficient of viscosity $K$.

No-slip and impermeability at the inclined surface $y=0$ are expressed by the boundary conditions (4), while the outer condition (5) assures that the velocity component $w_x$ within the boundary layer approaches the external velocity

$$w_{x,\infty}=\sqrt{2gx\cos\alpha} \tag{7}$$

at the edge $y=\delta_l$ of the momentum boundary layer. Since the frictionless flow between the viscous boundary layer and the free streamline bordering the constant-pressure atmosphere is quasi-one-dimensional, the simple solution (7) is readily derived from equation (2) by assuming $w_{x,\infty}=0$ (and infinite film thickness) at the inlet $x=0$, cf. Andersson and Irgens [11].

## 3. Similarity transformation

Incidently, as pointed out by Andersson and Irgens [11], the external velocity (7) belongs to the Falkner–Skan class of freestreams $w_{x,\infty}\propto x^m$ which permits a similarity transformation of the momentum boundary layer equation even for power-law fluids. A generalized Falkner–Skan type of transformation was therefore introduced in refs. [11, 12], while we [13] recently devised an alternative similarity transformation. However, as we shall see, exact similarity solutions of the thermal energy equation exist only in the particular case when the power-law index $n$ is equal to 1.

Introducing new independent and dimensionless variables

$$\eta=\frac{y}{x}(Re_x)^{1/(n+1)} \tag{8}$$

$$\xi=\frac{x}{L} \tag{9}$$

where $L$ is a characteristic length scale in the streamwise direction and

$$Re_x=\frac{x^n(w_{x,\infty})^{2-n}\rho}{K} \tag{10}$$

is a generalized local Reynolds number. We follow ref. [13] and define dimensionless velocity components:

$$W_x(\eta)=w_x/\sqrt{2gx\cos\alpha} \tag{11}$$

$$W_y(\eta)=(w_y/\sqrt{2gx\cos\alpha})(Re_x)^{1/(n+1)} \tag{12}$$

which become analogous to the similarity transformations used in refs. [14–17] for the particular parameter value $n=1$. Unlike the dimensionless velocity components $W_x$ and $W_y$, which are independent of $\xi$, the dimensionless temperature

$$\theta(\eta,\xi)=\frac{t-t_\infty}{t_w-t_\infty} \tag{13}$$

will depend both on $\eta$ and $\xi$. The partial differential equations (1)–(3) and their boundary conditions (4)–(6) are now transformed into the following set of dimensionless equations:

$$W_x(\eta)-\frac{n}{n+1}\eta\frac{dW_x(\eta)}{d\eta}+2\frac{dW_y(\eta)}{d\eta}=0 \tag{14}$$

$$W_x(\eta)\left(-\frac{n}{n+1}\eta\frac{dW_x(\eta)}{d\eta}+W_x(\eta)\right)+2W_y(\eta)\frac{dW_x(\eta)}{d\eta}=1+2n\left(\frac{dW_x(\eta)}{d\eta}\right)^{(n-1)}\frac{d^2W_x(\eta)}{d\eta^2} \tag{15}$$

$$\left[-\frac{n}{2(n+1)}\eta W_x(\eta)+W_y(\eta)\right]\frac{\partial\theta(\eta,\xi)}{\partial\eta}$$

$$+\xi W_x(\eta)\frac{\partial\theta(\eta,\xi)}{\partial\xi}=\frac{1}{\xi^{(n-1)/2(n+1)}Pr_L}\frac{\partial^2\theta(\eta,\xi)}{\partial\eta^2} \quad (16)$$

subject to the boundary conditions

$$\eta=0: \quad W_x(\eta)=0, \quad W_y(\eta)=0, \quad \theta(\eta,\xi)=1 \quad (17)$$

$$\eta=\eta_{\delta_t}: \quad W_x(\eta)=1 \quad (18)$$

$$\eta=\eta_{\delta_t}: \quad \theta(\eta,\xi)=0. \quad (19)$$

Here, the denominator ($\xi^{(n-1)/2(n+1)}\,Pr_L$) in the diffusion coefficient in equation (16) can be identified as the local Prandtl number

$$Pr_x=Re_x^{-2/(n+1)}\cdot\frac{xW_{x,\infty}}{a} \quad (20)$$

where $a$ is the thermal diffusivity $\lambda/\rho c_\rho$ and $Pr_L$ is the particular value of $Pr_x$ at the streamwise position $x=L$. Now, it is readily seen that $Pr_x\to 0$ as $x\to 0$ if $n>1$ and that $Pr_x\to\infty$ as $x\to 0$ if $n<1$.

In the special case when the power-law index $n$ is equal to unity, i.e. for a Newtonian liquid film, $Pr_x$ simplifies to $K/\rho a$. Since the diffusion coefficient in equation (16) then becomes independent of $x$, $\partial\theta/\partial\xi=0$ and similarity can be achieved also for the temperature field. This particular case has been explored by Andersson [24].

## 4. Solution of the hydrodynamical problem

It is noteworthy that the momentum boundary layer problem defined by the ordinary differential equations (14) and (15) subject to the relevant boundary conditions (17) and (18) is decoupled from the thermal boundary layer problem. The hydrodynamical problem was solved by Andersson and Shang [13] and accurate numerical similarity solutions were provided for several values of the power-law index in the range from 0.1 to 2.0. The computed velocity profiles $W_x(\eta)$ shown in Fig. 2 reveal that the power-law index has a substantial effect on the velocity distribution. As observed already by Andersson and Irgens [11], the most striking feature being the monotonic thinning of the momentum boundary layer with increasing $n$-values.

## 5. Solution of the heat transfer problem

### 5.1. The local nonsimilarity approach

Although the hydrodynamical problem admits similarity solutions, the accompanying thermal problem does not since the governing equation (16) for the temperature field exhibits explicit dependencies on both $\xi$ and $\eta$. An accurate method for obtaining locally nonsimilar boundary-layer solutions was suggested by Sparrow et al. [25]. According to [25] local nonsimilarity is achieved by first introducing the new variable $g(\eta,\xi)=\partial\theta/\partial\xi$ in the actual differential equation so that the energy equation (16) becomes

$$\left[-\frac{n}{2(n+1)}\eta W_x(\eta)+W_y(\eta)\right]\frac{\partial\theta(\eta,\xi)}{\partial\eta}$$

$$+\xi W_x(\eta)g(\eta,\xi)=\frac{1}{Pr_x}\frac{\partial^2\theta(\eta,\xi)}{\partial\eta^2}. \quad (21)$$

Differentiating equation (21) with respect to $\xi$, we have

$$\left[-\frac{n}{2(n+1)}\eta W_x(\eta)\right.$$

$$\left.+W_y(\eta)\right]g'(\eta,\xi)-W_x(\eta)g(\eta,\xi)+\frac{\partial g(\eta,\xi)}{\partial\xi}\xi W_x(\eta)$$

$$=\frac{1}{Pr_x}\left[g''(\eta,\xi)-\xi^{-1}\frac{n-1}{2(n+1)}\frac{\partial^2\theta(\eta,\xi)}{\partial\eta^2}\right] \quad (22)$$

where the primes have been introduced to denote differentiation with respect to $\eta$. The final step is to neglect terms involving $(\partial/\partial\xi)$ in the subsidiary equation (22), whereas the primary equation (16) remains intact. We introduce the new variable

$$h(\eta,\xi)\equiv\xi\cdot g(\eta,\xi)=\xi\,\partial\theta/\partial\xi \quad (23)$$

so that the subsidiary equation (22) simplifies to

$$\left[-\frac{n}{2(n+1)}\eta W_x(\eta)+W_y(\eta)\right]h'(\eta,\xi)+W_x(\eta)h(\eta,\xi)$$

$$=\frac{1}{Pr_x}\left[h''(\eta,\xi)-\frac{n-1}{2(n+1)}\frac{\partial^2\theta(\eta,\xi)}{\partial\eta^2}\right] \quad (24)$$

after multiplication by $\xi$. Likewise, $\xi g(\eta,\xi)$ in equation (21) is replaced by $h$. Thus, the two-equation local nonsimilarity model consists of the coupled second-order differential equations (21) and (24) for the two unknowns $\theta$ and $h$. These equations can be treated as ordinary differential equations and solved as a two-point boundary value problem in the single variable $\eta$ with $n$ and $Pr_x$ being the only parameters. Boundary conditions for the subsidiary unknown $h$ become

$$\eta=0: \quad h(\eta,\xi)=0 \quad (25)$$

$$\eta=\eta_{\delta_t} \quad h(\eta,\xi)=0 \quad (26)$$

after differentiation of the boundary conditions (17) and (19) for $\theta$ with respect to $\xi$.

### 5.2. Critical local Prandtl number $\mathrm{Pr}_x^*$

The thickness $\eta_{\delta_t}$ of the thermal boundary layer is generally different from the thickness $\eta_{\delta_1}$ of the momentum boundary layer. The latter depends only on the power-law index $n$ and it was observed in our preceding study [13] that $\eta_{\delta_1}$ was a monotonically decreasing function of

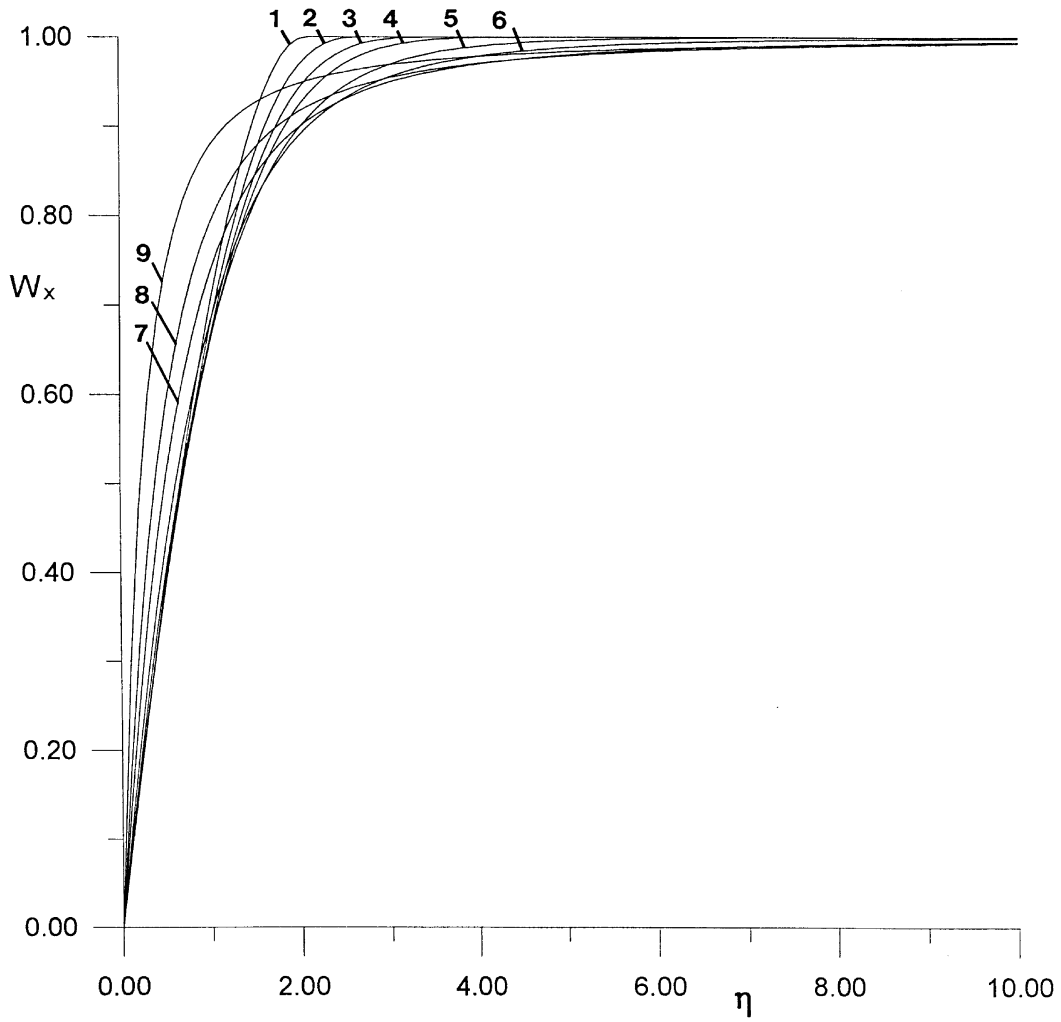


Fig. 2. Numerical similarity solutions for the streamwise velocity component $W_x(\eta)$. Curves 1–9: $n = 2.0$, 1.5, 1.2, 1.0, 0.7, 0.5, 0.3, 0.2, and 0.1.

$n$ throughout the parameter range $0.1 \leqslant n \leqslant 2.0$. In that study $\eta_{\delta_1}$ was defined in accordance with common practice in aerodynamic boundary layer theory, namely as the value of $\eta$ for which the dimensionless velocity component $W_x(\eta)$ becomes equal to 0.99. For convenience, however, in the present investigation $\eta_{\delta_1}$ is defined as the value of $\eta$ for which $W_x$ is practically equal to one (i.e. to within $10^{-4}$%) and denoted by $\eta^*$. The variation of $\eta^*$ with $n$ is displayed in Fig. 3.

Since the thickness of the thermal boundary layer is obtained as a part of the solution of a two-parameter problem, $\eta_{\delta_t}$ does not only depend on $n$ but varies also with $Pr_x$. For a given value of $n$, a critical value of the local Prandtl number is defined as the particular parameter value for which $\eta_{\delta_t}$ equals $\eta_{\delta_1}$. This critical value is denoted by $Pr_x^*$ and shown in Fig. 4, from which $Pr_x^*$ can be seen to increase monotonically with $n$.

### 5.3. *Precautions for* $\mathrm{Pr_x} > \mathrm{Pr_x^*}$

The thickness $\eta_{\delta_1}$ of the momentum boundary layer exceeds the thermal boundary layer thickness $\eta_{\delta_t}$ if $Pr_x > Pr_x^*$ and the difference between the two thicknesses increases with increasing $Pr_x$ so that the temperature gradients are only confined to the innermost part of the velocity boundary layer for $Pr_x \gg Pr_x^*$. The numerical accuracy will accordingly deteriorate if the two boundary layer problems are solved simultaneously all the way from the wall ($\eta = 0$) to the edge of the momentum boundary layer ($\eta = \eta_{\delta_1}$), cf. Table 1. The remedy is to

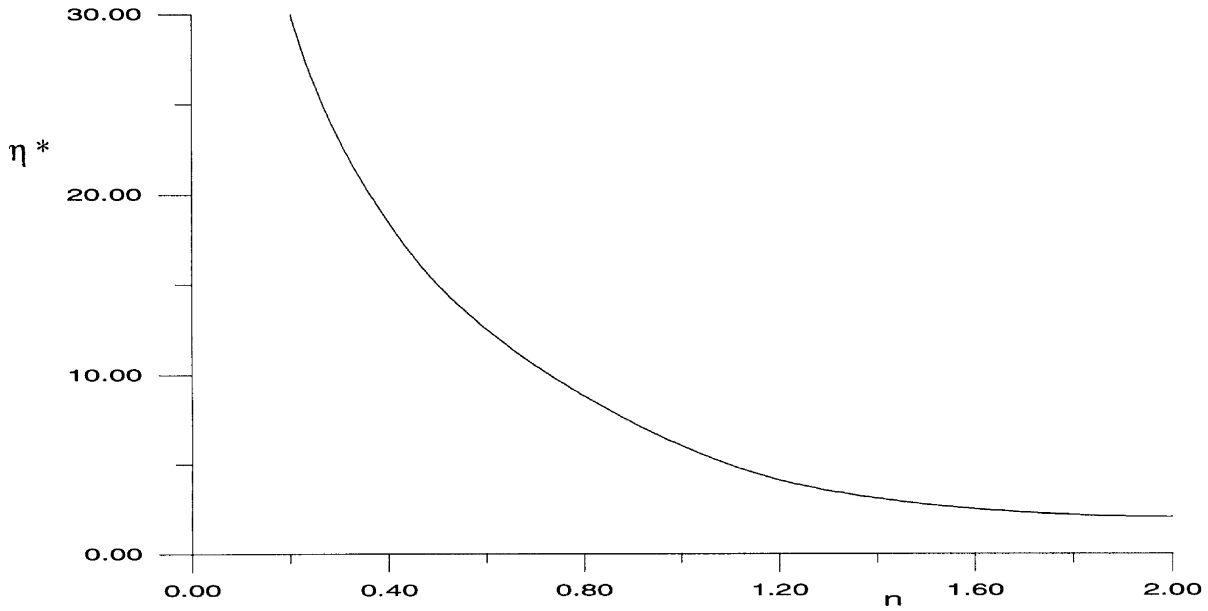


Fig. 3. Variation of dimensionless momentum boundary layer thickness $\eta^*$ with power-law index $n$.

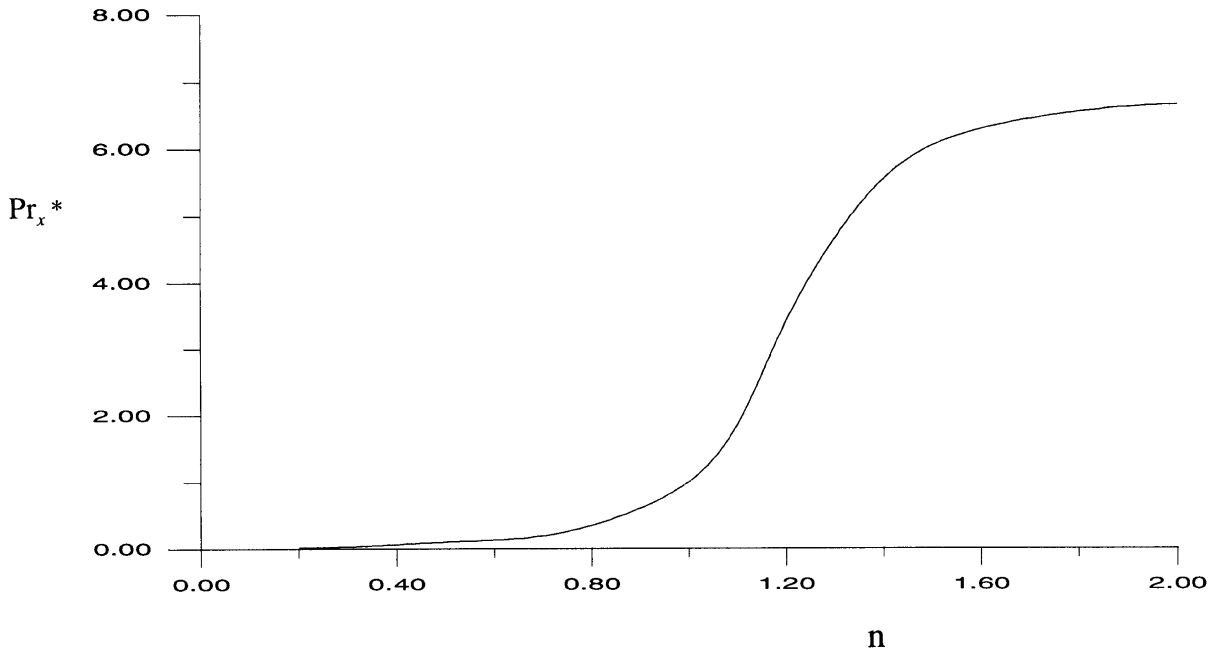


Fig. 4. Variation of critical local Prandtl number $Pr_x^*$ with power-law index $n$.

carry out the integration only sufficiently far so that the temperature gradient vanishes. To accomplish this, the external boundary condition for the velocity field in equation (18) is replaced with the accurately computed value of $W_x$ at the particular position which corresponds to the edge of the calculation domain for the temperature field. As for the specific example $n = 0.5$ and $Pr_x = 10$ in Table 2, the numerical solution was obtained with $W_x$

Table 1
Similarity solution for the velocity field for power-law index $n = 0.5$

| $\eta$ | $W_y$ | $W_x$ | $dW_x/d\eta$ |
|---|---|---|---|
| 0 | 0 | 0 | 1.104406 |
| 0.1 | −0.001811 | 0.105273 | 1.001948 |
| 0.2 | −0.007129 | 0.200581 | 0.905206 |
| 0.3 | −0.015776 | 0.286522 | 0.814695 |
| 0.4 | −0.027575 | 0.363738 | 0.730722 |
| 0.5 | −0.042347 | 0.432889 | 0.653416 |
| 0.6 | −0.059914 | 0.494642 | 0.582748 |
| 0.7 | −0.080097 | 0.549655 | 0.518561 |
| 0.8 | −0.102721 | 0.598562 | 0.460595 |
| 0.9 | −0.127614 | 0.64197 | 0.408512 |
| 1 | −0.154608 | 0.680448 | 0.361926 |
| 1.2 | −0.214262 | 0.744686 | 0.28355 |
| 1.4 | −0.280483 | 0.794992 | 0.222044 |
| 1.6 | −0.352205 | 0.83441 | 0.17416 |
| 1.8 | −0.428503 | 0.865373 | 0.137048 |
| 2 | −0.508594 | 0.889788 | 0.108331 |
| 2.2 | −0.591817 | 0.909136 | 0.086094 |
| 2.4 | −0.677629 | 0.924557 | 0.068834 |
| 2.5 | −0.721362 | 0.931076 | 0.061694 |
| 3 | −0.946498 | 0.955015 | 0.036572 |
| 3.5 | −1.179419 | 0.969477 | 0.022584 |
| 4 | −1.417354 | 0.978569 | 0.014495 |
| 4.5 | −1.658602 | 0.984503 | 0.009636 |
| 5 | −1.9021 | 0.988507 | 0.006611 |
| 5.5 | −2.147165 | 0.991292 | 0.004665 |
| 6 | −2.393348 | 0.99328 | 0.003375 |
| 7 | −2.887953 | 0.995822 | 0.001885 |
| 8 | −3.384437 | 0.99729 | 0.001132 |
| 9 | −3.882046 | 0.998198 | 0.000722 |
| 10 | −4.380367 | 0.998791 | 0.000484 |
| 11 | −4.879161 | 0.999198 | 0.00034 |
| 12 | −5.37828 | 0.999488 | 0.000248 |
| 13 | −5.877633 | 0.999704 | 0.000187 |
| 14 | −6.377156 | 0.999869 | 0.000146 |
| 15 | −6.876808 | 1 | 0.000118 |

$(2.5) = 0.931076$ taken from Table 1 as outer condition for $W_x$, in spite of the fact that the momentum boundary layer extends all the way to $\eta = 15$.

### 5.4. *Precautions for* $\mathrm{Pr_x} < \mathrm{Pr_x^*}$

The thermal boundary layer becomes thicker than the viscous boundary layer if $Pr_x < Pr_x^*$ and the ratio $\eta_{\delta_t}/\eta_{\delta_1}$ increases as $Pr_x$ is reduced. Temperature gradients thus extend far into the frictionless flow. To facilitate the numerical integration of the thermal boundary layer problem and assure the numerical accuracy, the momentum boundary layer equations (14) and (15) are integrated only up to $\eta_{\delta_1}$. Thereafter, the velocity field is taken as

$$W_x(\eta) = 1 \quad \text{and} \quad W_y(\eta) = -\tfrac{1}{2}\eta + \text{constant} \tag{27}$$

throughout the remaining $\eta$-range from $\eta_{\delta_1}$ to $\eta_{\delta_t}$. Here, with $W_x(\eta) = 1$ in the continuity equation (14), the explicit variation of $W_y(\eta)$ in (27) is readily obtained by straightforward integration. A specific example $n = 1.5$ and $Pr_x = 1$ is given in Table 3 and shown graphically in Fig. 5. Here, the analytical continuation in the range $2.7 \leqslant \eta \leqslant 5.6$ is represented by broken lines.

## 6. Numerical results

The above non-Newtonian flow and heat transfer problem was solved numerically for several values of the power-law index in the range $0.2 \leqslant n \leqslant 2.0$ for local Prandtl numbers $Pr_x$ from 0.001 to 1000. A number of computed temperature profiles are presented in Fig. 6, while the wall gradient, which is the most important heat transfer characteristic, is shown in Fig. 7. For the particular parameter value $n = 1$ the wall gradient data in Table 4 agreed in the fourth significant digit with the calculations for a Newtonian film by Andersson [24] throughout the entire Prandtl number range.

The most striking feature of Fig. 6 is that the Prandtl number effect is more prominent than the influence of the rheological parameter $n$. Irrespective of the value of the power-law index, the thickness of the thermal boundary layer is roughly the same as the thickness of the momentum boundary layer for $Pr_x = 1$. Moreover, for high Prandtl numbers the thermal layer is significantly thinner than the viscous layer, while for $Pr_x \ll 1$ the thermal boundary layer extends far into the external free stream. Consequently, the thinning of the thermal boundary layer with increasing values of $Pr_x$ makes the magnitude of the temperature gradient at the wall increase monotonically with the local Prandtl number, cf. Fig. 7. The thick thermal boundary layer in the low Prandtl number cases suggests that the temperature adjusts from $t_w$ to $t_\infty$ mainly in fluid with free stream velocity $w_{x,\infty}$. Thus, as a first approximation, the viscous boundary layer does not contribute to the heat flux and the temperature gradient at the wall should therefore be independent of $n$. However, the data for $Pr_x = 0.001$ in Table 4 show that the wall gradient increases slowly with $n$ as $n$ is varied from 0.2–2.0, the total increase being less than 8%. For $Pr_x \ll 1$ the principal effect of the viscous boundary layer on the temperature gradient at the wall stems from the displacement of the external inviscid flow away from the wall. As demonstrated by Andersson [26] the heat transfer rate is slightly overestimated if the displacement effect is neglected. Since the displacement thickness of the momentum boundary layer has been seen to decrease with increasing values of the power-law index [11], the observed wall gradients in Table 4 tend to increase slightly with $n$.

Table 2
Local nonsimilarity solution of the heat transfer problem for $n = 0.5$ and $Pr_x = 10$

| $\eta$ | $W_y$ | $W_x$ | $dW_x/d\eta$ | $\theta$ | $d\theta/d\eta$ |
|---|---|---|---|---|---|
| 0 | 0 | 0 | 1.104406 | 1.000000 | −1.139345 |
| 0.1 | −0.001811 | 0.105273 | 1.001948 | 0.886103 | −1.137857 |
| 0.2 | −0.007129 | 0.200581 | 0.905206 | 0.772716 | −1.127787 |
| 0.3 | −0.015776 | 0.286522 | 0.814695 | 0.661083 | −1.101675 |
| 0.4 | −0.027575 | 0.363738 | 0.730722 | 0.553101 | −1.054052 |
| 0.5 | −0.042347 | 0.432889 | 0.653416 | 0.451082 | −0.982272 |
| 0.6 | −0.059914 | 0.494642 | 0.582748 | 0.357429 | −0.887155 |
| 0.7 | −0.080097 | 0.549655 | 0.518561 | 0.274286 | −0.773095 |
| 0.8 | −0.102721 | 0.598562 | 0.460595 | 0.203198 | −0.647450 |
| 0.9 | −0.127614 | 0.64197 | 0.408512 | 0.144881 | −0.519255 |
| 1 | −0.154608 | 0.680448 | 0.361926 | 0.099129 | −0.397539 |
| 1.2 | −0.214262 | 0.744686 | 0.28355 | 0.040563 | −0.200474 |
| 1.4 | −0.280483 | 0.794992 | 0.222044 | 0.013642 | −0.081438 |
| 1.6 | −0.352205 | 0.83441 | 0.17416 | 0.003704 | −0.026229 |
| 1.8 | −0.428503 | 0.865373 | 0.137048 | 0.000799 | −0.006607 |
| 2 | −0.508594 | 0.889788 | 0.108331 | 0.000135 | −0.001286 |
| 2.2 | −0.591817 | 0.909136 | 0.086094 | 0.000017 | −0.000192 |
| 2.4 | −0.677629 | 0.924557 | 0.068834 | 0.000001 | −0.000022 |
| 2.5 | −0.721362 | 0.931076 | 0.061694 | 0.000000 | −0.000007 |

A qualitatively different situation occurs for high local Prandtl numbers. Due to the substantial thinning of the thermal boundary layer with increasing $Pr_x$, the temperature gradients are contained within the innermost part of the momentum boundary layer. Thus, the wall gradient of the temperature field is controlled by the velocity gradient $dW_x/d\eta$ at the wall. The accurate numerical solution of the hydrodynamic problem in [13] showed that $dW_x/d\eta$ is practically independent of $n$ for dilatant films but increases significantly with increasing pseudo-plasticity $1-n$ for $n < 1$. It is therefore interesting to observe that exactly the same $n$-dependency is carried over to the wall gradients of the temperature field in Table 4.

## 7. Heat transfer

The heat transfer rate between the solid wall which is maintained at temperature $t_w$ and the liquid film is of particular significance in industrial applications. The local heat transfer rate $q_x$, which is governed by Fourier's law, is conveniently expressed as a local heat transfer coefficient

$$a_x = \frac{q_x}{t_w - t_\infty} = -\lambda x^{-1} (Re_x)^{1/(n+1)} \left(\frac{\partial\theta(\eta,\xi)}{\partial\eta}\right)_{\eta=0} \tag{28}$$

or, alternatively, as a local Nusselt number

$$Nu_x = \frac{\alpha_x x}{\lambda} = -(Re_x)^{1/(n+1)} \left(\frac{\partial\theta(\eta,\xi)}{\partial\eta}\right)_{\eta=0}. \tag{29}$$

To facilitate rapid estimates of the local heat transfer coefficient $\alpha_x$ or the local Nusselt number $Nu_x$, accurate curve-fit formulas for the wall gradient of the temperature field

$$-\left(\frac{\partial\theta(\eta,\xi)}{\partial\eta}\right)_{\eta=0} = a + bPr_x^c \tag{30}$$

are provided. The optimised expressions for the coefficients $a$, $b$ and $c$, as obtained by matching the formula (30) to the data in Table 4, are given in Table 5. Predictions by means of this short-cut method are also included in Table 4 and turn out to compare accurately with the numerical results over the entire parameter ranges $0.2 \leqslant n \leqslant 2.0$ and $0.001 \leqslant Pr_x \leqslant 1000$.

## 8. Local similarity vs. local nonsimilarity

A simpler approach to the nonsimilar heat transfer problem associated with the gravity-driven power-law film would be the local similarity scheme. In that approach $\xi$ is regarded as a known constant at any streamwise position and the last term on the left-hand-side of equation (16) is, therefore, neglected. The numerical solution of the simplified version of equation (16) can then be obtained locally with $Pr_x$ and $n$ as parameters by means of the same integration technique as for the local nonsimilar problem defined in Section 5.1 and with the same precautions as described in Sections 5.3 and 5.4.

The two-parameter local similarity problem was solved

Table 3
Local nonsimilarity solution of the heat transfer problem for $n = 1.5$ and $Pr_x = 1.0$

| $\eta$ | $W_y$ | $W_x$ | $dW_x/d\eta$ | $\theta$ | $d\theta/d\eta$ |
|---|---|---|---|---|---|
| 0 | 0 | 0 | 0.865908 | 1 | −0.485194 |
| 0.1 | −0.000872 | 0.084788 | 0.829724 | 0.951482 | −0.485141 |
| 0.2 | −0.003513 | 0.165922 | 0.792848 | 0.902982 | −0.484778 |
| 0.3 | −0.007964 | 0.243336 | 0.755334 | 0.854547 | −0.483804 |
| 0.4 | −0.014265 | 0.316969 | 0.717243 | 0.806251 | −0.481941 |
| 0.5 | −0.022462 | 0.386768 | 0.678643 | 0.758197 | −0.478929 |
| 0.6 | −0.032598 | 0.452683 | 0.63961 | 0.710511 | −0.474537 |
| 0.7 | −0.044719 | 0.514678 | 0.600232 | 0.663342 | −0.468567 |
| 0.8 | −0.058871 | 0.572721 | 0.560604 | 0.616856 | −0.460861 |
| 0.9 | −0.075097 | 0.626794 | 0.520837 | 0.571231 | −0.451305 |
| 1 | −0.093438 | 0.676888 | 0.481052 | 0.526658 | −0.439837 |
| 1.2 | −0.136618 | 0.765174 | 0.401986 | 0.441431 | −0.411192 |
| 1.4 | −0.188649 | 0.837799 | 0.324677 | 0.362651 | −0.375526 |
| 1.6 | −0.249641 | 0.895264 | 0.250661 | 0.291595 | −0.334268 |
| 1.8 | −0.319506 | 0.938405 | 0.181772 | 0.22918 | −0.289483 |
| 2 | −0.397884 | 0.968456 | 0.120153 | 0.175877 | −0.24357 |
| 2.2 | −0.484046 | 0.987115 | 0.068278 | 0.131667 | −0.198916 |
| 2.4 | −0.57679 | 0.996604 | 0.028956 | 0.096088 | −0.157574 |
| 2.6 | −0.674316 | 0.999743 | 0.005337 | 0.068316 | −0.121037 |
| 2.7 | −0.724114 | 1 | 0.000493 | 0.057033 | −0.104856 |
| 2.8 | −0.774108 | 1 | 0 | 0.047296 | −0.090137 |
| 3 | −0.874108 | 1 | 0 | 0.03187 | −0.065079 |
| 3.4 | −1.074108 | 1 | 0 | 0.013323 | −0.030914 |
| 3.8 | −1.274108 | 1 | 0 | 0.004974 | −0.012972 |
| 4 | −1.374108 | 1 | 0 | 0.002909 | −0.008021 |
| 4.4 | −1.574108 | 1 | 0 | 0.000906 | −0.002794 |
| 4.8 | −1.774108 | 1 | 0 | 0.000243 | −0.000858 |
| 5 | −1.874108 | 1 | 0 | 0.000116 | −0.000454 |
| 5.4 | −2.074108 | 1 | 0 | 0.000016 | −0.000114 |
| 5.6 | −2.174108 | 1 | 0 | 0 | −0.000054 |

The velocity field beyond $\eta = 2.7$ is obtained from the analytical continuation in equation (27).

numerically for various combinations of $n$ and $Pr_x$ in the intervals $0.2 \leqslant n \leqslant 2.0$ and $0.001 \leqslant Pr_x \leqslant 1000$. Results for the magnitude of the wall gradient of the dimensionless temperature field, i.e. $-\partial\theta/\partial\eta|_{n=0}$ are reported in Table 4. To facilitate the comparison between the local nonsimilarity and the local similarity approach the deviation between the two sets of data, normalized with the latter, has been defined as $\varepsilon$ and included in the table.

Let us emphasize that the two approaches become identical for $n = 1$ since the thermal boundary layer problem admits exact similarity solutions for Newtonian fluids. It is therefore not surprising that the relative deviation $\varepsilon$ in the local similarity and local nonsimilarity solutions increases with deviation of the power-law index $n$ from unity, i.e. with increasing non-Newtonian rheology. The deviation is moreover more significant for the most pseudoplastic liquids ($n = 0.2$) than for the highly dilatant film ($n = 2.0$), whereas the local Prandtl number $Pr_x$ turned out to have only a minor effect on $\varepsilon$. The largest value of $\varepsilon$ for each $n$ is shown in Fig. 8. Since the local similarity solutions generally are in fairly close agreement with the more accurate local nonsimilarity solutions, their relative deviation never exceeding 9%, it is likely to conclude that the results obtained with the local nonsimilarity approach are of good accuracy.

## 9. Conclusions

This paper has focused on the heat transfer from an inclined plane surface to an accelerating liquid film of a power-law fluid. Although the thermal boundary layer equation generally fails to permit similarity solutions, a novel similarity transformation devised by Andersson and Shang [13] for the accompanying hydrodynamical problem was adopted in combination with a local non-

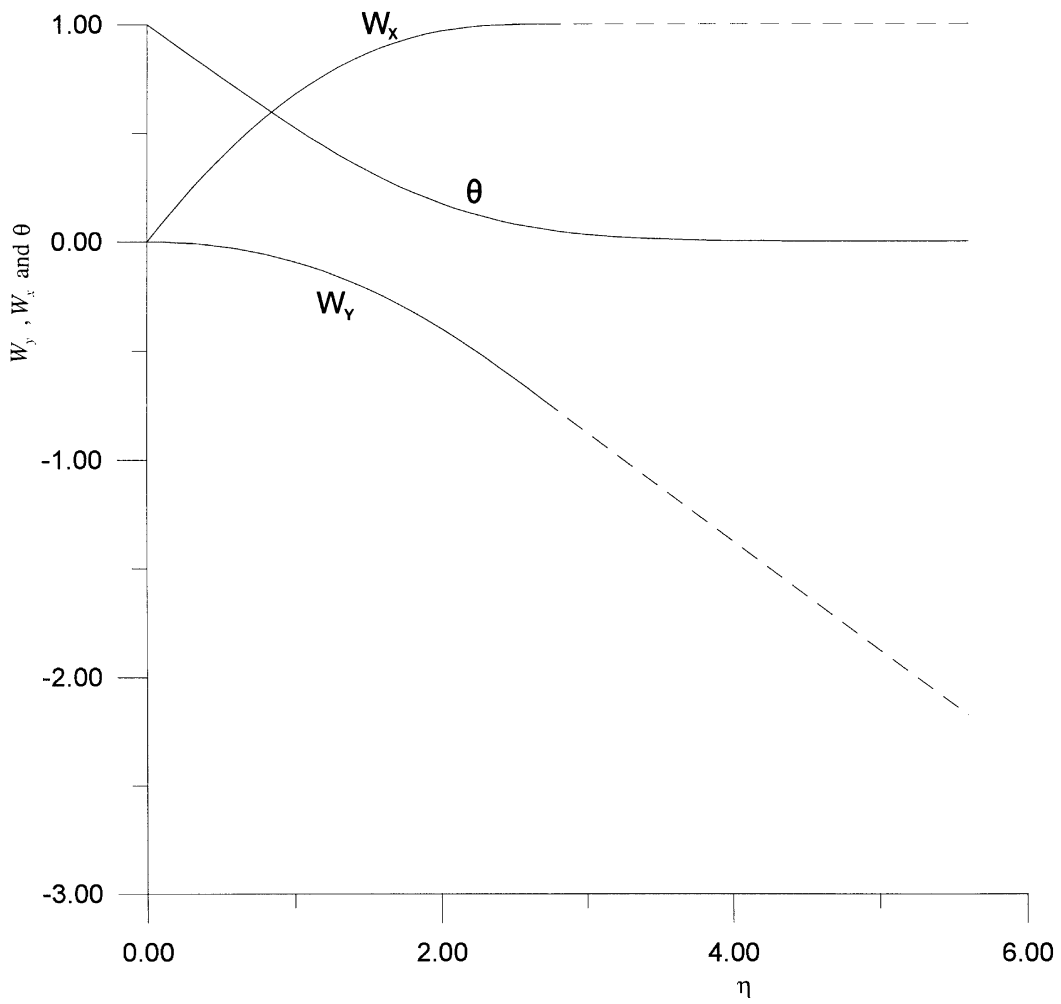


Fig. 5. Profiles of dimensionless temperature $\theta$ and velocity components $W_x$ and $W_y$ for $n = 1.5$ and $Pr_x = 1.0$. Solid lines represent numerical results and broken lines denote the analytical continuations in equation (27).

similarity solution method due to Sparrow et al. [25]. The resulting transformed problem turned out to involve only two independent parameters, namely the power-law index $n$ and the local Prandtl number $Pr_x$ defined in equation (20). It is noteworthy that all other parameters, like the streamwise location $x$, the fluid properties $\varrho$, $K$, $n$, $c_\rho$ and $\lambda$ and the component of the gravitational acceleration along the wall $g\cos\alpha$, have been combined into $Pr_x$ and the local Reynolds number $Re_x$ in equation (10). Accurate numerical results were obtained for various combinations of $Pr_x$ and $n$ covering the range of Prandtl numbers from 0.001–1000 and for the power-law index in the range $0.2 \leqslant n \leqslant 2.0$. Special treatment of the low and high Prandtl number cases was essential in order to maintain the numerical accuracy and the results were practically indistinguishable from those of Andersson [24] for $n = 1$ over the entire $Pr_x$-range. The main findings can be summarized as follows:

(1) The thickness of the thermal boundary layer decreases monotonically with increasing $Pr_x$. The thermal boundary layer extends far out in the free stream for $Pr_x \ll 1$ and is on the other hand confined to the innermost part of the momentum boundary layer for $Pr_x \gg 1$.
(2) The local heat transfer coefficient and the local Nusselt number depend on the local Reynolds number $Re_x$ and the wall gradient of the dimensionless temperature.
(3) For $Pr_x \gg 1$ the wall temperature gradient is controlled by the velocity gradient at the wall, which was practically independent of $n$ for dilatant fluids

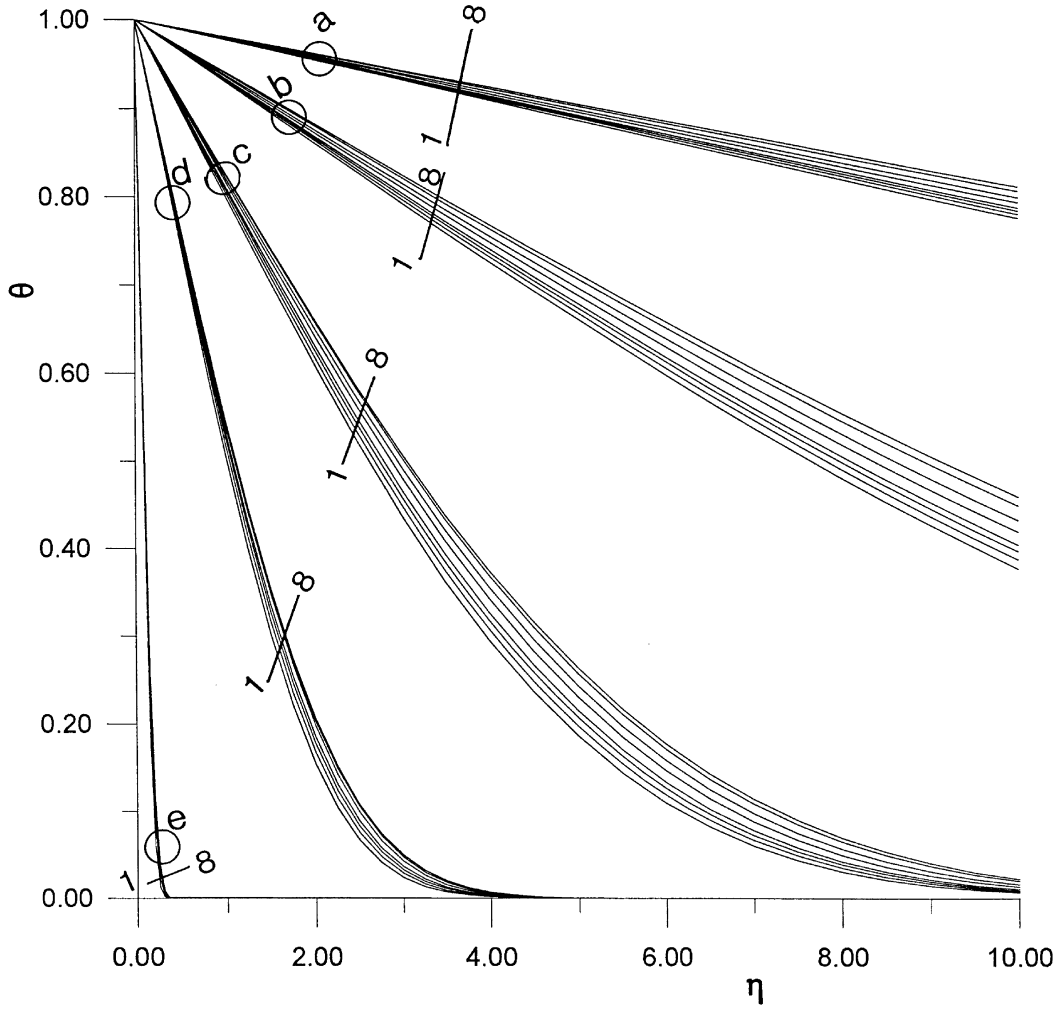


Fig. 6. Local nonsimilarity solutions for the dimensionless temperature profile $\theta(\eta)$ for different values of the local Prandtl number $Pr_x$ and the power-law index $n$: (a) $Pr_x = 0.001$; curves 1–8: $n = 0.2$, 0.3, 0.5, 0.7, 1.0, 1.2, 1.5 and 2.0. (b) $Pr_x = 0.01$; curves 1–8: $n = 0.2$, 0.3, 0.5, 0.7, 1.0, 1.2, 1.5 and 2.0. (c) $Pr_x = 0.1$; curves 1–8: $n = 0.2$, 0.3, 0.5, 0.7, 1.0, 1.2, 1.5 and 2.0. (d) $Pr_x = 1.0$; curves 1–8: $n = 2.0$, 1.5, 1.2, 1.0, 0.2, 0.7, 0.3 and 0.5. (e) $Pr_x = 1000$; curves 1–8: $n = 0.2$, 0.3, 2.0, 0.5, 1.5, 0.7, 1.2 and 1.0.

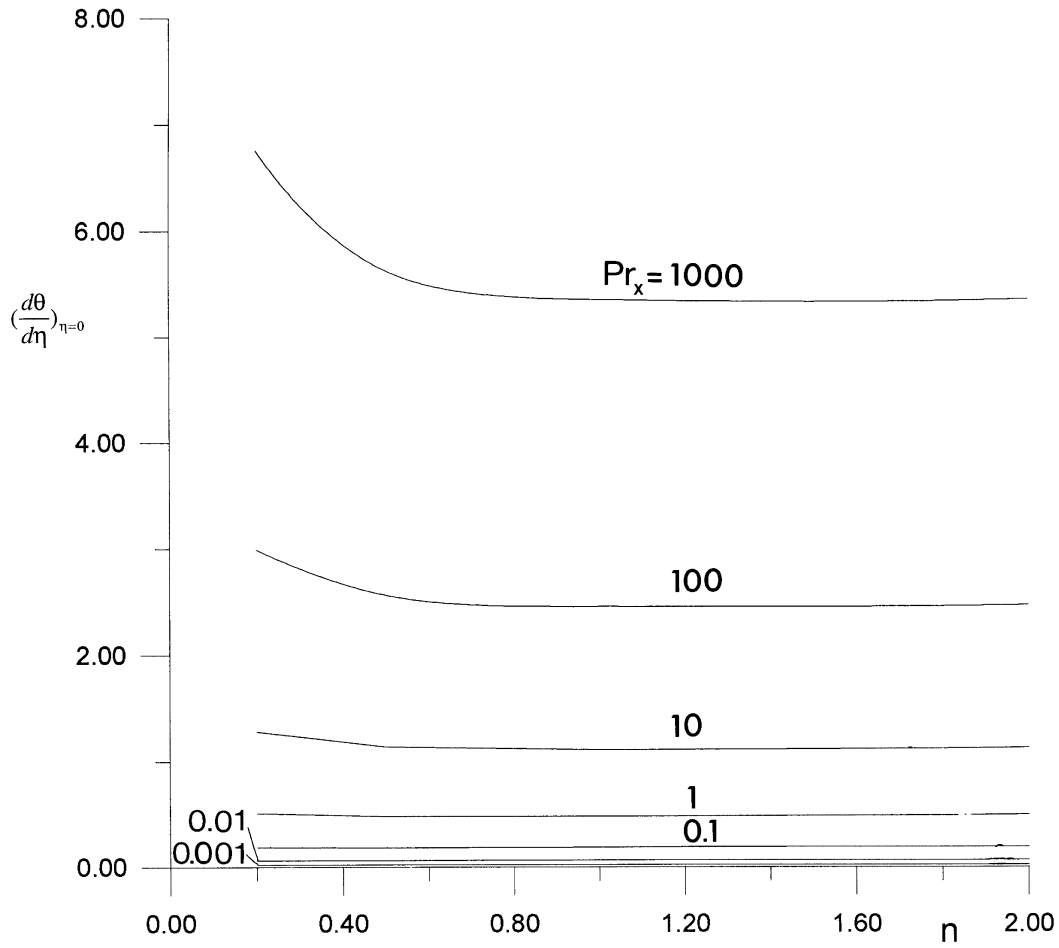


Fig. 7. Variation of dimensionless temperature gradient $\partial\theta/\partial\eta$ at the wall $\eta = 0$ with power-law index $n$ for different values of the local Prandtl number $Pr_x$.

Table 4
Computed values of the temperature gradient $\partial\theta/\partial\eta$ at the wall $\eta = 0$ for different values of the local Prandtl number $Pr_x$ and the power-law index $n$

| $n$ | | $Pr_x$ | | | | | | |
|---|---|---|---|---|---|---|---|---|
| | | 0.001 | 0.01 | 0.1 | 1 | 10 | 100 | 1000 |
| 0.2 | (1) | 0.020533 | 0.063147 | 0.186309 | 0.511085 | 1.279857 | 2.988850 | 6.759796 |
| | (2) | 0.020781 | 0.064269 | 0.183771 | 0.512150 | 1.281350 | 2.986210 | 6.759290 |
| | (3) | 0.018972 | 0.058368 | 0.172436 | 0.474205 | 1.192632 | 2.786635 | 6.237978 |
| | (4) | 8.23% | 8.19% | 8.04% | 7.78% | 7.31% | 7.26% | 8.36% |
| 0.5 | (1) | 0.020969 | 0.063909 | 0.183605 | 0.479263 | 1.139345 | 2.564116 | 5.628706 |
| | (2) | 0.020792 | 0.064943 | 0.179742 | 0.478240 | 1.136410 | 2.459580 | 5.639690 |
| | (3) | 0.020222 | 0.061618 | 0.177284 | 0.463786 | 1.105026 | 2.490641 | 5.473721 |
| | (4) | 3.69% | 3.72% | 3.57% | 3.34% | 3.11% | 2.95% | 2.83% |
| 0.7 | (1) | 0.021202 | 0.064578 | 0.184728 | 0.475799 | 1.115688 | 2.491717 | 5.455400 |
| | (2) | 0.021161 | 0.065951 | 0.181193 | 0.477702 | 1.115440 | 2.493870 | 5.468850 |
| | (3) | 0.020810 | 0.063356 | 0.181350 | 0.468008 | 1.098647 | 2.454498 | 5.371625 |
| | (4) | 1.88% | 1.93% | 1.86% | 1.66% | 1.55% | 1.52% | 1.56% |
| 1.0 | (1) | 0.021457 | 0.065358 | 0.186817 | 0.477573 | 1.106714 | 2.454025 | 5.351840 |
| | (2) | 0.021458 | 0.066731 | 0.182300 | 0.477310 | 1.102480 | 2.449260 | 5.351000 |
| | (3) | 0.021455 | 0.065358 | 0.186817 | 0.477573 | 1.106714 | 2.454025 | 5.351840 |
| | (4) | 0% | 0% | 0% | 0% | 0% | 0% | 0% |
| 1.2 | (1) | 0.021595 | 0.065830 | 0.188319 | 0.480393 | 1.107689 | 2.448439 | 5.330138 |
| | (2) | 0.021601 | 0.067153 | 0.183434 | 0.480264 | 1.105269 | 2.448156 | 5.336428 |
| | (3) | 0.021786 | 0.066408 | 0.189943 | 0.484187 | 1.115816 | 2.466169 | 5.370314 |
| | (4) | −0.88% | −0.87% | −0.85% | −0.78% | −0.73% | −0.72% | −0.75% |
| 1.5 | (1) | 0.021763 | 0.066406 | 0.190326 | 0.485268 | 1.112966 | 2.451963 | 5.329753 |
| | (2) | 0.021788 | 0.067760 | 0.185113 | 0.484680 | 1.109650 | 2.450740 | 5.331060 |
| | (3) | 0.022179 | 0.067674 | 0.193864 | 0.493425 | 1.130459 | 2.489701 | 5.412861 |
| | (4) | −1.88% | −1.87% | −1.82% | −1.65% | −1.55% | −1.52% | −1.54% |
| 2.0 | (1) | 0.022111 | 0.067165 | 0.192984 | 0.492759 | 1.124601 | 2.468207 | 5.356678 |
| | (2) | 0.022099 | 0.068771 | 0.187911 | 0.492040 | 1.120480 | 2.467170 | 5.356030 |
| | (3) | 0.022654 | 0.069220 | 0.198848 | 0.506364 | 1.153169 | 2.529702 | 5.490155 |
| | (4) | −2.40% | −2.97% | −2.95% | −2.69% | −2.48% | −2.43% | −2.43% |

(1) Local similarity solutions.
(2) Accurate curve-fit formula equation (30).
(3) Local nonsimilarity solutions.
(4) Relative deviation between local nonsimilarity and local similarity results normalized with the latter.

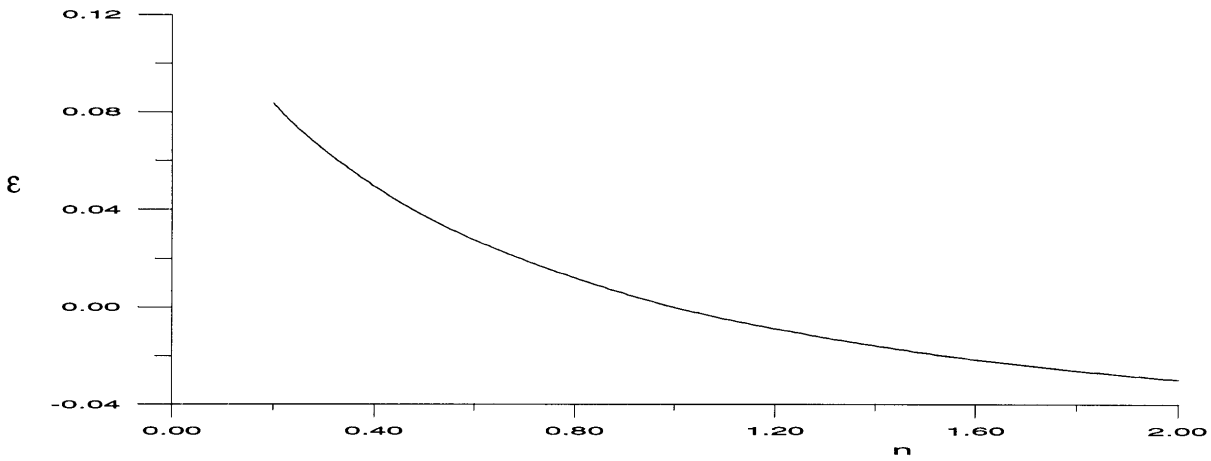


Fig. 8. Largest relative deviation $\varepsilon$ between local nonsimilarity and local similarity solutions in the wall gradient $\partial\theta/\partial\eta$. Variation with power-law index $n$.

Table 5
Coefficients $a$, $b$ and $c$ in the curve-fit formula (30) for low ($Pr_x \leqslant 1$) and high ($Pr_x \geqslant 1$) local Prandtl numbers and for pseudoplastic ($n \leqslant 1$) and dilatant ($n \geqslant 1$) fluids

| |
|---|
| For $0.001 \leqslant Pr_x \leqslant 1$ |
| $a = -0.0086 + 0.0009 \times (1/n)$ |
| $b = 0.485 + 0.00001 \times (1/n)^{1/n}$ |
| $c = 0.399 + 0.008 \times (1/n)$ |
| $(0.2 \leqslant n \leqslant 1)$ |
| $a = -0.0074 - 0.00028n$ |
| $b = 0.47 + 0.015n$ |
| $c = 0.407$ |
| $(1 \leqslant n \leqslant 2)$ |
| For $1 \leqslant Pr_x \leqslant 1000$ |
| $a = 0.0205 - 0.0845(1/n)^{1/3}$ |
| $b = 0.518 + 0.0234(1/n)$ |
| $c = 0.3324 + 0.00096(1/n)^{1.6}$ |
| $(0.2 \leqslant n \leqslant 1)$ |
| $a = -0.12 + 0.079[n/(n+1)]^{1/2}$ |
| $b = 0.541 + 0.0009n^3$ |
| $c = 0.3306 + 0.0027(1/n)^{1.65}$ |
| $(1 \leqslant n \leqslant 2)$ |

($n > 1.0$) but increased significantly with increasing pseudo-plasticity ($1-n$).

(4) For $Pr_x \ll 1$ the temperature gradient increased slightly with $n$ and this modest variation was ascribed to the displacing influence of the momentum boundary layer on the external frictionless flow.

(5) Finally, a set of accurate curve-fit formulas for the wall temperature gradient is provided in order to enable rapid estimates of the heat transfer rate for any combination of $n$ and $Pr_x$ within the parameter ranges considered.

A special case of the transformation used herein has previously been applied in the analysis of the heat transfer in Newtonian liquid films with variable fluid properties [16, 17]. The successful generalization to non-Newtonian fluids makes us believe that the present approach should be applicable also to the analysis of heat transfer in power-law films with variable thermophysical properties.

## Acknowledgement

This study was partly supported by the Research Council of Norway under Contract Nos 110657/410 and 119182/410.

## References

[1] H.I. Andersson, The momentum integral approach to laminar thin-film flow, ASME Symposium on Thin Fluid Films, Cincinnati, OH, FED-48 (1987) 7–13.
[2] G. Astarita, G. Marrucci, G. Palumbo, Non-Newtonian gravity flow along inclined plane surfaces, Ind. Eng. Chem. Fundam. 3 (1964) 333–339.
[3] N. Therien, B. Coupal, J.L. Corneille, Verification expérimentale de l'épaisseur du film pour des liquides non-Newtoniens s'écoulant par gravité sur un plan incliné, Can. J. Chem. Eng. 48 (1970) 17–20.
[4] N.D. Sylvester, J.S. Tyler, A.H.P. Skelland, Non-Newtonian thin films: theory and experiment, Can. J. Chem. Eng. 51 (1973) 418–429.
[5] T.M.T. Yang, D.W. Yarbrough, A numerical study of the laminar flow of non-Newtonian fluids along a vertical wall, ASME J. Appl. Mech. 40 (1973) 290–292.
[6] T.M.T. Yang, D.W. Yarbrough, Laminar flow of non-Newtonian liquid films inside a vertical pipe, Rheol. Acta 19 (1980) 432–436.

[7] V. Narayana Murthy, P.K. Sarma, A note on hydrodynamics entrance lengths of non-Newtonian laminar falling liquid films, Chem. Eng. Sci. 32 (1977) 566–567.
[8] V. Narayana Murthy and P.K. Sarma, Dynamics of developing laminar non-Newtonian falling liquid films with free surface, ASME J. Appl. Mech. 45 (1978) 19–24.
[9] M.N. Tekic, D. Posarac, D. Petrovic, A note on the entrance region lengths of non-Newtonian laminar falling films, Chem. Eng. Sci. 41 (1986) 3230–3232.
[10] H.I. Andersson, F. Irgens, Hydrodynamic entrance length of non-Newtonian liquid films, Chem. Eng. Sci. 45 (1990) 537–541.
[11] H.I. Andersson, F. Irgens, Gravity-driven laminar film flow of power-law fluids along vertical walls, J. Non-Newtonian Fluid Mech. 27 (1988) 153–172.
[12] H.I. Andersson, F. Irgens, Film flow of power-law fluids, in: N.P. Cheremisinoff (Ed.), Encyclopedia of Fluid Mechanics, vol. 9, Gulf Publishing, Houston, TX, 1990, pp. 617–648.
[13] H.I. Andersson, D.Y. Shang, An extended study of the hydrodynamics of gravity-driven film flow of power-law fluids, Fluid Dyn. Res. 22 (1998) 345–357.
[14] D.Y. Shang, B.X. Wang, Effect of variable thermophysical properties on laminar free convection of gas, Int. J. Heat Mass Transfer 33 (1990) 1387–1395.
[15] D.Y. Shang, B.X. Wang, Y. Wang, Y. Quan, Study on liquid laminar free convection with consideration of variable thermophysical properties, Int. J. Heat Mass Transfer 36 (1993) 3411–3419.
[16] D.Y. Shang, B.X. Wang, L.C. Zhong, A study on laminar film boiling of liquid along isothermal vertical plates in a pool with consideration of variable thermophysical properties, Int. J. Heat Mass Transfer 37 (1994) 819–828.
[17] D.Y. Shang, B.X. Wang, An extended study on steady-state laminar film condensation of a superheated vapour on an isothermal vertical plate, Int. J. Heat Mass Transfer 40 (1997) 931–941.
[18] S.M. Yih, M.W. Lee, Heating or evaporation in the thermal entrance region of a non-Newtonian laminar falling liquid film, Int. J. Heat Mass Transfer 29 (1986) 1999–2002.
[19] G. Astarita, Mass transfer from a flat solid surface to a falling non-Newtonian liquid film, Ind. Eng. Chem. Fundam. 5 (1966) 14–18.
[20] R.A. Mashelkar and V.V. Chavan, Solid dissolution in falling films of non-Newtonian liquids, J. Chem. Eng. Japan 6 (1973) 160–167.
[21] V.C. van der Mast, S.M. Read, L.A. Bromley, Boiling of natural sea water in falling film evaporators, Desalination 18 (1976) 71–94.
[22] V. Narayana Murthy and P.K. Sarma, Heat transfer to non-Newtonian laminar falling liquid films with smooth wave free gas–liquid interface, Int. J. Multiphase Flow 4 (1978) 413–425.
[23] H.I. Andersson, Forced convection heat transfer in accelerating laminar non-Newtonian films, Proceedings of the Fourth Asian Congress of Fluid Mechanics, Hong Kong 1 (1989) H1–H4.
[24] H.I. Andersson, Diffusion from a vertical wall into an accelerating falling liquid film, Int. J. Heat Mass Transfer 30 (1987) 683–689.
[25] E.M. Sparrow, H. Quack, C.J. Boerner, Local non-similarity boundary-layer solutions, AIAA J. 8 (1970) 1936–1942.
[26] H.I. Andersson, On approximate formulas for low Prandtl number heat transfer in laminar wedge flows, Int. J. Heat Fluid Flow 9 (1988) 241–243.